Proceedings of IMECE 2004
2004 ASME International Mechanical Engineering Congress and RD&D Expo
Anaheim, California, USA, November 13-19, 2004

IMECE2004-60363

TEMPERATURE-DEPENDENT LUMINESCENCE QUENCHING IN RANDOM NANO POROUS MEDIA

Xiulin Ruan and Massoud Kaviany*
Department of Mechanical Engineering
University of Michigan
Ann Arbor, Michigan 48109-2125
xruan@umich.edu, kaviany@umich.edu

ABSTRACT

The luminescence quenching of a random, crystalline one-dimensional model porous medium doped with rare-earth elements, is analyzed by considering the transport, transition, and interaction of the fundamental energy carriers. The quenching in nano porous media is enhanced compared to a single crystal, due to multiple scattering, enhanced absorption, and low thermal conductivity. The coherent wave treatment is used to calculate the photon absorption, in order to allow for field interference and enhancement. The luminescent and thermal emission is considered as incoherent. The luminescence quenching and nonlinear thermal emission, occurring with increasing irradiation intensity, are predicted.

NOMENCLATURE

c_o speed of light in vaccum (m/s)
c_p constant pressure specific heat capacity (J/kg-K)
c_v constant volume specific heat capacity (J/kg-K)
E complex electric field (V/m)
H complex magnetic field (A/m)
I intensity (W/m^2)
k wave vector (1/m), thermal conductivity (W/m-K)
l index of the layers
m_f, m_s complex refractive index of fluid, solid
N number of layers, number of phonons
N_2 electronic concentration at the excited state (1/m^3)
n_f, n_s refractive index of fluid, solid
$\mathbf{q}$ heat flux vector(W/m^2)
$\dot{s}$ volumetric energy conversion (W/m^3)
T temperature (K)

Greek symbols

γ decay rate (1/s)
ε permittivity (F/m)
ε porosity
η luminescent quantum yield
κ_s index of extinction of solid
λ wavelength (m)
λ_f gas mean free path (m)
λ_p phonon mean free path (m)
μ permeability (H/m)
σ_a absorption coefficient (1/m)
ω angular frequency (rad/s)

Subscripts

b blackbody
e emission, electron
f, s fluid, solid
l luminescent
k conductive
nr non-radiative
o free space
p phonon
ph photon
r radiative

*Address all correspondence to this author.

t thermal
0 resonant, incident frequency ω_0

INTRODUCTION

Luminescence quenching is typically a result of the thermo-optical bistability, in which the irradiated solid has two distinct responses depending on the increase or decrease in irradiation, caused by the temperature dependence of the optical and thermal properties [**?**]. This has relevance in switching applications in optical communications [**?**, **?**], and is of potential use in logic and memory systems for optical computations [**?**]. Recently, applications also include solid state lasers. Kuditcher et al. [**?**] reported bistable output in a Tm-doped glass waveguide laser when varying the incident pump intensity. Noginov et al. [**?**] observed similar results in Cr-doped lasers and laser materials. The temperature-dependent thermal and optical properties are among bistability factors creating a positive feedback with temperature. Consider an index of extinction which increases exponentially with temperature. A small increase in the irradiation intensity causes a proportional increase in absorption, as a result, the sample temperature is raised, causing a further increase in the index of extinction and a large absorption. This is the key mechanism in the thermal runaway and bistability in microwave heating [**?**, **?**]. Other temperature-dependent thermal and optical properties can also be responsible for bistability phenomena. For example, temperature-dependent thermal expansion is employed to manufacture thermo-optical switches [**?**]. Temperature-dependent luminescence quantum yield and thermal conductivity were responsible for the generation of a bistable blackbody radiator [**?**].

The bistability phenomena in nano porous media are of interest, due to their multiple scattering, low thermal conductivity, and radiative trapping properties. Lawandy [**?**] observed laser-like emission from laser dye solutions containing microparticles, for a promising novel laser system now collectively called "random laser". The scattering is thought to create closed paths, or loops, around which the light propagates and becomes amplified in the presence of a population inversion [**?**]. Rare earth doped solids are noted for their use as high power laser materials, as visible emitting phosphors in displays, and as constituents of Er-doped amplifiers in fiber optic systems for telecommunications.

Most of the bistability investigations have been qualitative, and the quantitative analyses of the onset of thermo-optical bistability were performed using a macroscopic, lumped energy conservation equation. Typical treatments are the "surface" and the "bulk" treatments [?, ?]. In the former, the absorption, luminescence and thermal emission are assumed to take place only at the surface. In the latter, the absorption is assumed to be lumped and the sample has a uniform temperature. Empirical or fitting parameters are used in both treatments. However, the volumetric absorption occurs over a large portion of the penetration depth in a sample with small extinction coefficient and small size. As a result, the temperature may vary much through the sample and cannot be assumed uniform, therefore affecting the sample absorption and emission.

In this study, the luminescence quenching of a random, crystalline multilayer doped with rare-earth elements, is analyzed, by considering the transport, transition, and interaction of the basic energy carriers. The coherent wave treatment (Maxwell's equations) is used to calculate the photon absorption, where field enhancement and size dependent absorption coefficient are observed. Particularly, the non-radiative decay is identified as a multiphonon relaxation process, and is highly temperature dependent, resulting in luminescence quantum yield rapidly decaying with increase in temperature. The luminescence quenching and nonlinear thermal emission, occurring with increase in irradiation, are then predicted. The luminescence quenching predicted here is continuous and not a sudden jump that would occur in onset of bistability. The proper conditions for having bistability in this rare-earth doped system is under investigation.

Theoretical Analysis

1 Interaction and transport physics

To understand the bistability at a microscopic level, the interaction and transport of basic energy carriers must be analyzed. The interaction mechanisms among the photon, electron, and phonon in ytterbium doped yttria are shown in Fig. **??**. The process of luminescence in rare earth systems starts with the absorption of energy on 4f-4f transitions by electrons, which are normally forbidden but are rendered by crystal field mixing. The excited electron often decays non-radiatively by emitting several phonons through a multiphonon relaxation process to a close, lower-lying level before emitting a photon to return to the ground state. The emitted photon is consequently of less energy than the initially absorbed energy and some heating takes place. The energy spectra of the incident and luminescent photons ($E_{ph,0}$ and $E_{ph,l}$), the excited and ground state electrons of Yb^{3+} (E_e), and the optical phonons in yttria (E_{ph}), are shown in Fig. **??**. These will be discussed in details in Sections 2, 3, and 4. The relative amount of heating is determined by the quantum efficiency η, which is the ratio of energy radiated to energy absorbed. Generally, η is a nonlinear function of temperature. Through these interactions, some photons of the incident frequency disappear, while photons of the luminescent frequency are generated, along with some phonons. Electrons are fermions so they cannot be generated or destroyed. However, the population at a particular (excited or ground) state can change by photon/phonon absorption and decay. These interactions provide sources or sinks for the three fundamental energy carriers.

The carrier transports need to be treated in addition to their sources and sinks. For photons, we treat them in a classical regime using Maxwell's equations to allow for the coherent inter-

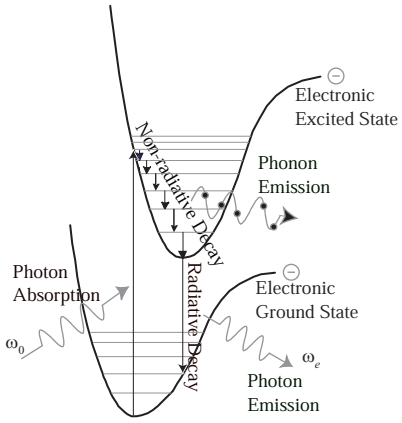

Figure 1. Interaction among photon, electron and phonon: photon absorption and emission, electron excitation and decay, and phonon emission

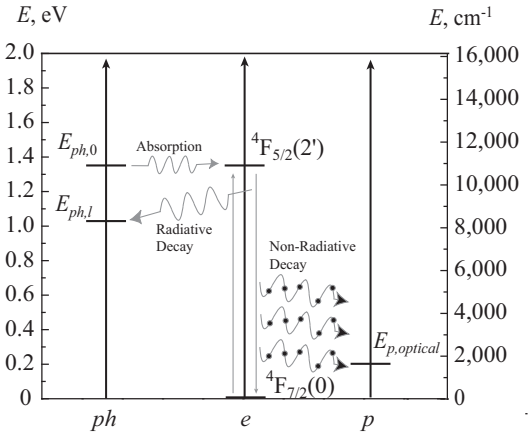

Figure 2. Energy spectra of the incident (0) and luminescent (l) photons (ph), excited and ground state electrons (e), and optical phonons (p), for $Yb:Y_2O_3$. The various transitions are also shown.

ference effects. Since electrons are bounded to ions and no free electrons are present, we neglect their movement and just consider their transition between the excited and ground states. For phonons, we use the non-radiative decay and Fourier conduction law, while including the size effect in nano multilayers.

2 Coherent photon absorption

Absorption occurs when the incident field couples to the dipole moment of the atom. This atom-field interaction is strongest as the incident light is tuned on resonance of the electronic transition, which is the case in this analysis. Generally the index of extinction is used to describe the absorbing ability of a

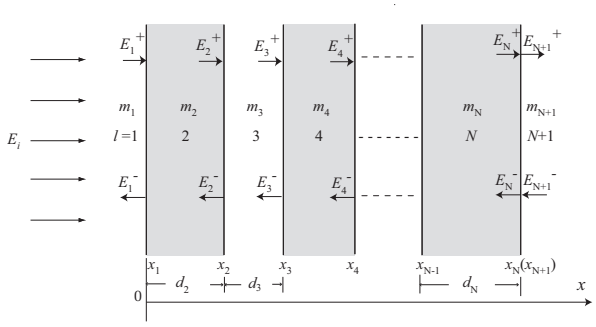

Figure 3. Model nano porous medium, parallel solid and fluid layers with random thickness. The porosity is prescribed.

material. To treat the absorption as a volumetric behavior, the local field amplitude needs to be determined first.

The simplest model of a random porous medium consists of parallel solid layers with random thickness, as shown in Fig. **??**. Regions $l=1$ and $N+1$ are semi-infinite media of air. This multilayer medium has $N/2$ (N is an even number here) solid layers and $N/2-1$ air layers. The coordinates $x_1, x_2, ..., x_N$ are chosen such that the thickness of each layer is random, but obeys a trapezoidal distribution. This multilayer medium has a finite dimension in the direction of the electromagnetic wave propagation x, and an infinite length in the plane normal to x. The dielectric solid material has a complex refractive index $m_{s,\omega}(=n_{s,\omega}+i\kappa_{s,\omega})$ which depends on the electromagnetic wave frequency. In this section, all the quantities and parameters are at the incident frequency ω_0, and thus the subscript ω_0 is omitted for convenience. The air has a refractive index $m_f(=n_f=1)$.

The general theory starts with Helmholtz's equation

$$\frac{\partial^2 E(x)}{\partial x^2} + k_o^2 m^2 E(x) = 0, \tag{1}$$

where k_o is the vacuum wave vector, and m is the local complex index of refraction at the incident frequency. This is the electromagnetic wave equation in a source-free medium, and is equivalent to Maxwell's equations in the multilayer system. For the medium shown in Fig. **??**, the solution of Eq. (**??**) at a particular location in the l-th layer is given by

$$E(x) = E_l^+ e^{ik_l(x-x_l)} + E_l^- e^{-ik_l(x-x_l)},\ l = 1,2,...,N+1, \tag{2}$$

where x_{N+1} takes the value of x_N since there are only N interfaces and $k_l = m_l\omega_0/c_o$ is the wave vector, where ω_0 is the angular frequency of the incident radiation and c_o is the speed of light in vacuum. The field in the medium is divided into two components, the forward (transmitted) component E_l^+ and the backward (reflected) component E_l^-. The boundary conditions require that

the tangential electric and magnetic fields be continuous across each interface. The relationship between the amplitudes of the l-th and (l+1)-th interfaces are given in the matrix form [**?**]

$$\begin{pmatrix} E_l^+ \\ E_l^- \end{pmatrix} = D_l^{-1} D_{l+1} P_{l+1} \begin{pmatrix} E_{l+1}^+ \\ E_{l+1}^- \end{pmatrix}, \; l = 1,2,...,N, \qquad (3)$$

where

$$D_l = \begin{pmatrix} 1 & 1 \\ m_l & -m_l \end{pmatrix}, \; l = 1,2,...,N+1, \qquad (4)$$

and D_l^{-1} is the inverse of D_l, and

$$P_l = \begin{pmatrix} e^{-ik_l(x_l - x_{l-1})} & 0 \\ 0 & e^{ik_l(x_l - x_{l-1})} \end{pmatrix}, \; l = 2,3,...,N+1. \qquad (5)$$

Hence

$$\begin{pmatrix} E_j^+ \\ E_j^- \end{pmatrix} = \begin{pmatrix} M_{11}^{(j)} & M_{12}^{(j)} \\ M_{21}^{(j)} & M_{22}^{(j)} \end{pmatrix} \begin{pmatrix} E_{N+1}^+ \\ E_{N+1}^- \end{pmatrix}, \; j = 1,2,...,N, \qquad (6)$$

where

$$\begin{pmatrix} M_{11}^{(j)} & M_{12}^{(j)} \\ M_{21}^{(j)} & M_{22}^{(j)} \end{pmatrix} = \prod_{l=j}^{N} D_{l-1} D_{l+1} P_{l+1}, \; j = 1,2,...,N. \qquad (7)$$

For a wave incident from medium 1, we have $E_{N+1}^- = 0$. Therefore,

$$\frac{E_j^+}{E_1^+} = \frac{M_{11}^{(j)}}{M_{11}^{(1)}} \qquad (8)$$

and

$$\frac{E_j^-}{E_1^+} = \frac{M_{21}^{(j)}}{M_{11}^{(1)}}. \qquad (9)$$

The use of Eqs. (**??**) and (**??**) in Eq. (**??**) yields the field everywhere. The magnetic field is given by [**?**]

$$\mathbf{H}(x) = \frac{1}{i\omega_0 \mu} \nabla \times \mathbf{E}(x), \qquad (10)$$

where μ is the magnetic permeability.

In order to determine the distribution of the power absorbed inside the layers, the power flux must be determined. The Poynting vector is

$$I(x) = |\overline{\mathbf{S}}(x)| = \frac{1}{2} |\mathrm{Re}[\mathbf{E}(x) \times \mathbf{H}^*(x)]|. \qquad (11)$$

The local energy conversion rate due to the absorption at the resonance frequency is [**?**]

$$\dot{s}_0(x) = -\frac{\partial I_0(x)}{\partial x} = \frac{2\pi n_l \kappa_l}{\lambda} \left(\frac{\varepsilon_o}{\mu_o} \right)^{\frac{1}{2}} |E(x)|^2, \qquad (12)$$

where ε_o and μ_o are the free space permittivity and permeability.

3 Rate equation for electrons

The rate equations describe population dynamics of statistically independent atoms. They are not, however, completely correct when used to describe atoms with any correlations between them, such as in cooperative interactions or other interatomic couplings. In the nanopowders studied, observation of any cooperative effects is negligible [**?**]. In steady state, the excitation rate from the ground state is balanced by the decay rate from the excited state, and the population of the excited state remains constant with respect to time. The steady-state rate equation is

$$\frac{dN_2}{dt} = \frac{\dot{s}_0(x)}{\hbar\omega_0} - \gamma(T) N_2 = 0, \qquad (13)$$

where N_2 is the electronic concentration at the excited state, and $\gamma(T)$ is the temperature-dependent decay rate.

4 Non-radiative and radiative decay

In addition to radiative decays, there can be other mechanisms collectively termed non-radiative. When working with rare-earth elements, the predominant mechanisms are phonon-assisted energy transfer and multiphonon relaxation. Phonon-assisted energy transfer is a non-resonant energy transfer process in which the mismatch of energy between the level of the sensitizer and the activator is compensated by the simutaneous emission or absorption of one or more phonons. Multiphonon relaxation is decay to a lower level by the emission of two or more phonons. Emission of phonons will lead to internal heating of the system. Miyakawa and Dexter proposed a theory to describe both processes [**?**].

The non-radiative decay is through a multiphonon relaxation process, and is governed by the "energy gap law" or

"phonon number law". In measurements on $Yb:Y_2O_3$, the non-radiative decay is modeled as a multiphonon process. This is a temperature-dependent rate and the theoretical expression can be given by

$$\gamma(T) = \gamma(T=0)\left[1-\exp\left(\frac{-\bar{h}\omega}{k_B T}\right)\right]^{-N}, \tag{14}$$

where $\gamma(T=0)$ is the decay rate at absolute zero temperature, k_B is the Boltzmann constant, $\bar{h}\omega$ is the energy per phonon, and N is the number of phonons.

The decay rate given in Eq. (**??**) is the sum of the radiative and non-radiative decay rates. The radiative decay rate is usually assumed to be temperature independent. The non-radiative decay rate is temperature dependent, because it is a multiphonon relaxation process and the availability of phonon modes are temperature dependent. At absolute zero temperature, no non-radiative decay exists. The radiative and non-radiative decay rates are thus given by

$$\gamma_r = \gamma(T=0) \tag{15}$$

and

$$\gamma_{nr}(T) = \gamma(T) - \gamma_r. \tag{16}$$

The energy conversion rate due to the luminescence emission is given by

$$\dot{s}_l = -\gamma_r N_2 \bar{h}\omega_e, \tag{17}$$

where ω_e is the average luminescent frequency.

Using Eq. (**??**) in Eq. (**??**), $\dot{s}_l$ is written in a more explicit form

$$\dot{s}_l(x) = -\frac{\omega_e}{\omega_0}\eta\dot{s}_0(x) \tag{18}$$

where η is the luminescent quantum yield and is defined as

$$\eta = \frac{\gamma_r}{\gamma(T)}. \tag{19}$$

5 Thermal emission

Thermal emission always exists when an object is above absolute zero temperature, and the spectral blackbody emissive power is given by the Plank law. At low temperatures, thermal emission is small, and the detected emission is mainly the rare-earth luminescence. However, at high temperatures, the thermal emission becomes dominant. There have been several reports of blackbody emission of nanopowders at high temperatures. Costa et al. [**?**] investigated the emission features of silicon nanopowder. The powders were treated as independent blackbody radiators, and the total emission is calculated as the sum of their individual emissions. The emission spectrum was detected at high temperature and was verified to be a blackbody spectra. Redmond et al. [?] treated the thermal emission of yttria nanopowders as a surface phenomenon, and the experimentally detected emission spectrum was also demonstrated to be a blackbody spectrum.

It has not been clear in the literature as how this weakly absorbing material ($\kappa_{s,\omega_0} \sim 10^{-5}$) reveals a blackbody behavior. Here for simplicity we treat the multilayer system as an effective medium with homogeneous properties, and thus the scattering can be neglected. Assuming that the medium is a gray body, and the absorption coefficient is wavelength independent, the equation of radiative transfer can then be written as [**?**]

$$\frac{dI_{t,\lambda}}{dx} = -\sigma_{a,\lambda}I_{t,\lambda} + \sigma_{a,\lambda}I_{b,\lambda}, \tag{20}$$

where $I_{t,\lambda}$ is the spectral intensity of thermal emission, $\sigma_{a,\lambda}$ is the spectral absorption coefficient, and $I_{b,\lambda}$ is the blackbody emission intensity, given by Plank's law.

Eq. (**??**) is integrated from $x=0$ to x, starting from an initial intensity $I_{t,\lambda}(0)=0$, and this yields [?]

$$I_{t,\lambda}(x) = I_{t,\lambda}(x=0)\exp(-\sigma_{a,\lambda}x) + I_{b,\lambda}[1-\exp(-\sigma_{a,\lambda}x)]. \tag{21}$$

In the multilayer system, the initial thermal emission intensity $I_{t,\lambda}(x=0)$ is zero, and Eq. (**??**) is simplified to

$$I_{t,\lambda}(x) = I_{b,\lambda}[1-\exp(-\sigma_{a,\lambda}x)]. \tag{22}$$

To obtain the total thermal emission intensity, an integration over all the wavelength is to be performed on Eq. **??**. Recognizing that the spectral absorption coefficient is wavelength dependent, an average absorption coefficient $\bar{\sigma}_a$ which is not dependent on wavelength can be defined, such that the total thermal emission intensity is the same as that using the spectral absorption. Physically, yttria is considered as transparent at all wavelength except for the transition resonances, however, absorption always exists for all wavelength due to defects or impurities, et, al. Here, for simplicity the average absorption coefficient is taken as 1/10 of that of the resonance absorption. The total thermal emission is

$$I_t(x) = I_b[1-\exp(-\bar{\sigma}_a x)], \tag{23}$$

where I_b is the total emissive power given by the Stefan-Boltzmann law. It is clear that if the medium is optically thick ($\bar{\sigma}_a L$ is large), the collected emission at the surface ($x = L$) is nearly a blackbody spectrum.

The derivative of the total thermal emission intensity gives the local energy conversion rate due to thermal emission, i.e.,

$$\dot{s}_t(x) = -\frac{dI_t}{dx} = -\bar{\sigma}_a I_b \exp(-\bar{\sigma}_a x). \tag{24}$$

6 Heat conduction

Temperature is a critical parameter that governs thermo-optical bistability. For one-dimensional, steady-state heat conduction, the divergence of the conduction heat flux vector is given by the Fourier conduction law

$$\nabla \cdot \mathbf{q}_k = \nabla \cdot [k(T) \nabla T], \tag{25}$$

where $k(T)$ is treated as a temperature dependent thermal conductivity. Here, the sample temperature varies from room temperature (300 K) to the melting temperature of yttria (2,683 K). The thermal conductivities of yttria and air both change significantly in this range [**?**]. Additionally, when the thickness of the gas or solid layer is nearly the same as or smaller than the gas or phonon mean free path, the size effect must be considered. There are simple, approximation expressions describing this effect. One of the models that is used to predict the size dependence occurring in gas is [**?**]

$$k_f(T, d_f) = \frac{k_f(T)}{1 + \frac{4a_1(2-\gamma)}{\gamma(c_p/c_v+1)} Kn_{d_f}}, \tag{26}$$

where a_1 is a semi-empirical constant, $0 \leq \gamma \leq 1$ is the accommodation factor, and Kn_{d_f} is the Knudsen number defined as

$$Kn_{d_f} = \frac{\lambda_m}{d_f}, \tag{27}$$

and λ_m is given by

$$\lambda_m = \frac{1}{2^{1/2}} \frac{k_B T}{d_m^2 p}, \tag{28}$$

where d_m is the gas molecule collision diameter, and p is the pressure.

The solid layer-thickness dependence of the thermal conductivity of the solid layers may also be approximated as [?]

$$k_s(T, d_s) = \frac{k_s(T)}{1 + \frac{4}{3} \frac{\lambda_p}{d_s}}, \tag{29}$$

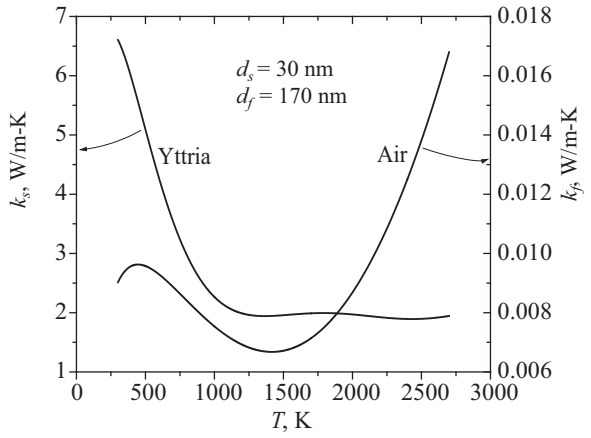

Figure 4. The solid and gas thermal conductivites as a function of temperature, with the size effect in nanoscale considered.

where $k_s(T)$ is the bulk solid thermal conductivity, and λ_p is the phonon mean free path. The predicted thermal conductivities of the gas and solid layers, using Eqs. (**??**) and (**??**), are plotted in Fig. **??**.

7 Energy conservation

The last step in completion of the theoretical model is to utilize the energy conservation equation by realizing that the sum of the divergence of the conduction and radiation heat flux vectors should be zero, i.e.,

$$\nabla \cdot (\mathbf{q}_k + \mathbf{q}_r) = 0, \tag{30}$$

where the divergence of the radiative heat flux vector is equal to the volumetric energy conversion due to photon absorption, luminescent and thermal emission, i.e.,

$$\nabla \cdot \mathbf{q}_r = \dot{s}_r = \dot{s}_0 + \dot{s}_l + \dot{s}_t. \tag{31}$$

Thus Eq. (**??**) can be rewritten in a more explicit form by using the result of Eqs. (**??**) and (**??**), i.e.,

$$\frac{d}{dx}\left[k(T)\frac{dT}{dx}\right] + \dot{s}_r(x, T) = 0, \tag{32}$$

with the boundary conditions being

$$T = T_0,\ x = x_N;\ \frac{dT}{dx} = 0,\ x = 0. \tag{33}$$

Equation **??** is a nonlinear equation for T, as the variables $k(T)$ and $\dot{s}_r(x,T)$ are both temperature dependent. The finite-volume method is used, and the converged solutions are obtained.

Results and discussion

1 Field enhancement and penetration depth

The above analysis is performed on myltilayer systems to predict their luminescent and thermal emission variations with respect to irradiation intensity. The parameters and properties used in the simulation is listed in Table 1. The local electric field component at the irradiation frequency is determined for a normal incident electromagnetic wave of wavelength $\lambda = 906$ nm, for the one-dimensional random medium with 5,000 solid layers with thickness d_s following a trapezoidal distribution between $\langle d_s \rangle \pm \Delta d_s = 30 \pm 10$ nm, and with a porosity $\langle \varepsilon \rangle = 0.85$, and $n_{s,\omega_0} = 1.8$, and $\kappa_{s,\omega_0} = 1.2 \times 10^{-5}$. The index of refraction n_{s,ω_0} is attributed to the yttria host, and the index of extinction κ_{s,ω_0} attributed to the ytterbium dopant. The dopant concentration is $4.1 \times 10^{20}\text{cm}^{-3}$, and the absorption cross section is $0.4 \times 10^{-20}\text{cm}^2$. Thus the spectral absorption coefficient of crystal is

$$\sigma_{a,\omega_0,c} = 4.1 \times 10^{20}\ \text{cm}^{-3} \times 0.4 \times 10^{-20}\ \text{cm}^2 = 1.64\ \text{cm}^{-1}, \quad (34)$$

and κ_{s,ω_0} is given by

$$\kappa_{s,\omega_0} = \frac{\sigma_{a,\omega_0,c}\lambda_0}{4\pi} = 1.2 \times 10^{-5}. \quad (35)$$

Table 1: Parameters and properties for simulation of luminescence quenching.

average porosity	$\langle \varepsilon \rangle$	0.85
incident wavelength	λ_0	906 nm
luminescent wavelength	λ_l	1,200 nm
solid layer mean thickness	$\langle d_s \rangle$	30 nm
solid layer thickness spread	Δd_s	10 nm
number of solid layers	$N/2$	5,000
index of refraction for solid	n_s	1.8
index of extinction for solid	κ_s	1.2×10^{-5}
ambient temperature	T_0	300 K
optical phonon energy	E_{ph}	1635 cm^{-1}
radiative decay rate	γ_r	955 1/s
absorption coefficient for thermal emission	$\overline{\sigma}_a$	16,666 1/m

There are infinite possible realizations for this model composite, and the field results for one of them are shown in Fig. **??**. As evident, there is a field enhancement, i.e., there is a peak in the field inside the medium and this peak can be much larger than the incident field, in most realizations [?]. In periodic porous media, the field is also periodic, resulting in no isolated peaks inside the media (even if the field in this case can also be higher than the incident field). The physical basis of field enhancement is electromagnetic wave interference. In this random multilayer system, the waves will multiply transmit and reflect at all the interfaces, and interfere with each other. At some location for some realization, the interference is so ideally constructive that it results in an extremely large field. Thus this large field enhancement is solely attributed to random porous structure, and cannot be observed in homogeneous or periodic media. Note that the coherence condition (the medium size is smaller than the coherence length) must be satisfied to observe the field enhancement. The coherence length is $\lambda^2/\Delta\lambda$ for a central wavelength λ and a spectrum width $\Delta\lambda$ [**?**]. In this study we use a monochromatic wave, thus satisfying the coherence condition ($\Delta\lambda$ is zero and coherence length infinite). The coherence length of many lasers is several kilometers, satisfying the coherence condition.

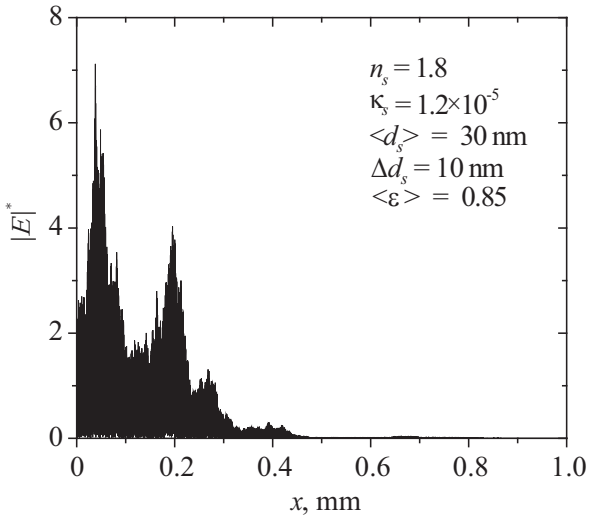

Figure 5. Typical Distribution of dimensionless field in nano porous medium with $L = 1$ mm. $|E|^*$ is normalized against the incident field.

It is interesting to notice that the penetration depth begins to depend on the sample size L for this random multilayer. The penetration depth is defined as the distance where the intensity decays to $1/e$ of the initial intensity. To investigate the expectation intensity decay profile of a sample, the intensity profiles of a large number of realizations with the same L are calculated and the ensemble average are made. Shown in Fig. **??** is the expectation decay profile of the dimensionless intensity of samples with the thickness 0.2, 0.4 and 0.6 mm, respectively. It is evident that initially the intensity decays exponentially, and then decays much slower. This is because the near surface region has a stronger coherent interference effect and thus a larger absorption. As a result of the presence of the slow decay region, the penetra-

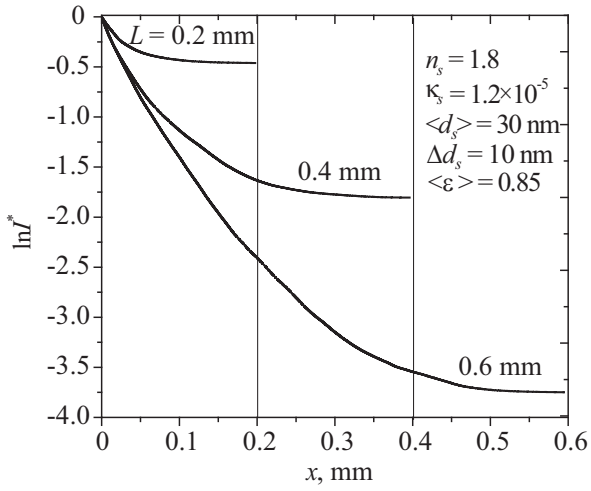

Figure 6. The decay of the dimensionless intensity with respect to x coordinate in samples with the thickness 0.2, 0.4 and 0.6 mm, respectively. The dimensionless intensity I^* is defined as $I^* = I(x)/I(x=0)$.

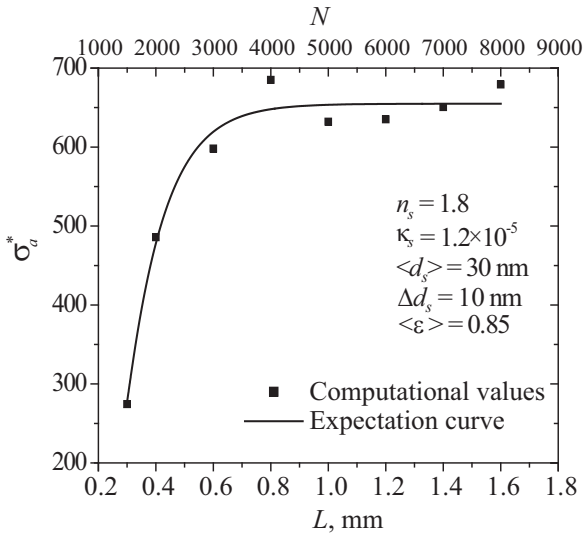

Figure 7. The variation of the dimensionless absorption coefficient with respect to the sample size. The dimensionless absorption coefficient σ_a^* is defined as $\sigma_a^* = \sigma_a / \left[\frac{4\pi\kappa}{\lambda}(1-\langle\varepsilon\rangle)\right]$.

tion depth becomes sample size dependent. A very thin film has a larger penetration depth, because the exponential decay region is too small, and the slow decay region moves towards the surface. As the film thickness increases, the penetration depth decreases and finally approaches a constant value, because the exponential decay region is large enough. The absorption coefficient of the multilayer is the reciprocal of the penetration depth, and is normalized against the crystal values to get the dimensionless absorption coefficient. This is shown in Fig. **??**. As expected, it is smaller in thin samples, and approaches a constant value as the sample is thick enough.

2 Luminescence quenching and thermal emission

Using the theoretical model developed above, the steady state temperature distribution, luminescent and thermal emission can be calculated given the irradiation intensity. Before this can be done, the temperature dependence of the non-radiative decay rate $\gamma_{nr}(T)$ needs to be determined. The lifetime measurements [?] suggest that the non-radiative decay is a 6 phonon relaxation process, with the energy of 1635 cm^{-1} per phonon. However, this is not clear , since the optical phonon of yttria have not yet been fully measured or analyzed (e.g., MD),although part of the phonon spectrum was given in [**?**]. As discussed, since the absorption of incident radiation occurs non-uniformly with the multi-layer system, the resulting temperature distribution is different from those predicted using a surface or a uniform treatment. This is shown in Fig. **??**, showing the surface treatment results in a higher surface temperature and the bulk (or uniform) treatment results in a much lower surface temperature.

The variations of the surface temperature, luminescent and

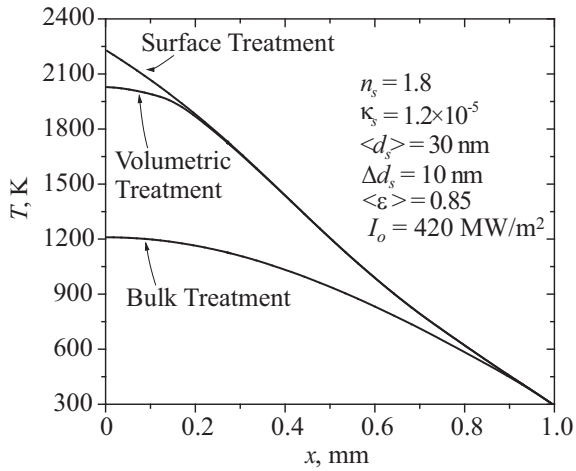

Figure 8. The predicted temperature distribution using surface, volumetric, and bulk treatments.

thermal emission intensities, with respect to the irradiation intensities, are shown in Figs. **??** and **??**. It is clear that initially the luminescent emission increases linearly with temperature, and then experiences a quenching. This is due to the temperature dependence of the luminescent quantum yield. The initial linear increase in I_l is indicated by Eq. (**??**), because the luminescent quantum yield η defined in Eq. (**??**) is a weak function of T at low temperatures, and $\dot{s}_o$ is proportional to the irradiation. In contrast at high temperatures the decay rate increases rapidly

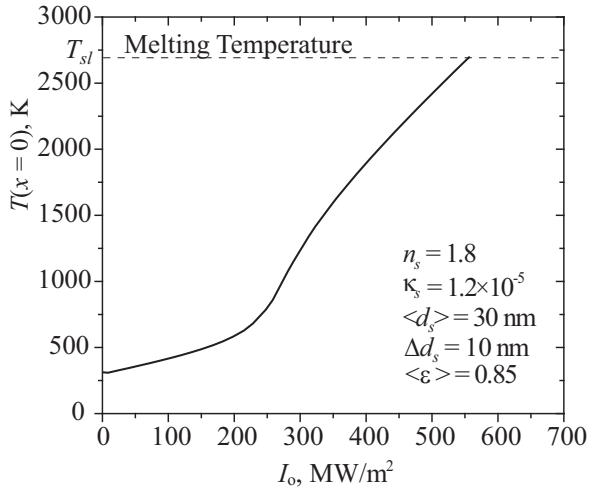

Figure 9. The variation of the surface temperature with respect to irradiation intensity.

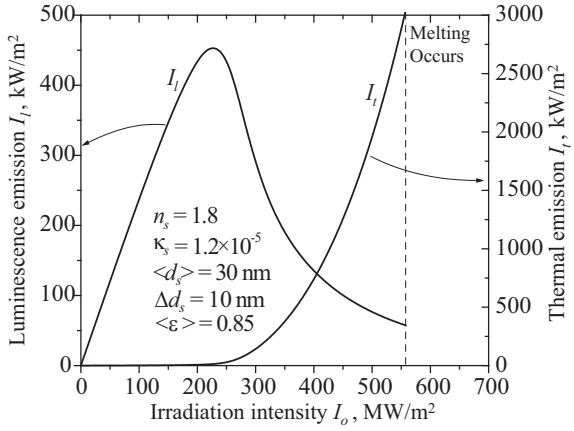

Figure 10. The variation of the luminescent and thermal emission intensities with respect to irradiation intensity.

with the temperature, and η is also a rapidly decaying function of temperature. Thus the luminescence emission is quenched. The thermal emission ia a blackbody spectrum, and is proportional to T^4, causing the emission intensity to increase rapidly at high irradiations. It should be noted that melting occurs when the melting temperature is reached. At the phase transition, the surface temperature will take a sudden jump to a higher stable state, because the reflection of the liquid phase is not as large as the solid multilayer. Then the thermal emission is considered "bistable".

CONCLUSIONS

A consistent model is developed to analyze the intrinsic thermo-optical bistability of random multilayer systems, by considering the interaction, transition, and transport of basic energy carriers. The coherent wave treatment is used for the photon absorption, and field enhancement and size dependnent penetration depth are predicted. The non-radiative decay is identified as a multiphonon relaxation process, and the luminescent quantum yield is highly temperature dependnent, causing the luminescence quenching. Qualitative agreement is found with the luminescent and thermal emissions of irradiated nanopowder [**?**].

ACKNOWLEDGEMENT

The support of Rackham School of Graduate Studies/Vice President for Research, The University of Michigan, through a research grant, is greatly appreciated. Discussions with Professor Stephen Rand have been very helpful and are greatly appreciated.

REFERENCES

[1] Gibbs, H.M., 1985, *Optical Bistability: Controlling Light with Light*, Academic Press, Orlando.

[2] Feng, S.T., and Irene, E.A., 1992, "Thermal-optical switching in Si based etalons", *J. Appl. Phys.*, **72**, (9), 3897-3903.

[3] Hoffmann, M., Kopka, P., Grob, T., and Voges, E., 1998, "All-silicon bistable micromechanical fibre switches", *Electronics Letters*, **34**, (2), 207-208.

[4] Boussekou, A., Molnar, G., Demont, P., and Menegotto, J., 2003, "Observation of a thermal hysteresis loop in the dielectric constant of spin crossover complexes: towards molecular memory devices", *J. Mat. Chem.*, **34**, 2069-2071.

[5] Kuditcher, A., Hehlen, M.P., Florea, C.M., Winick, K.W., and Rand, S.C., 2000, "Intrinsic bistability of luminescence and stimulated emission in Yb- and Tm-doped glass", *Phys. Rev. Lett.*, **84**, (9), 1898-1901.

[6] Noginov, M.A., Vondrova, M., and Lucas, B.D., 2001, "Thermal induced optical bistability in Cr-doped Colquiriite crystals", *Phys. Rev. B*, **65**, (3), 035112.

[7] Vriezinga, C.A., 1995, "Thermal runaway and bistability in microwave heated isothermal slabs", *J. Appl. Phys.*, **79**, (3), 1779-1783.

[8] Alpert, Y., and Jerby, E., 1999, "Coupled thermal-electromagnetic model for microwave heating of temperature-dependent dielectric media", *IEEE Transactions on Plasma Science*, **27**, (2), 555-562.

[9] Hoffmann, M., Kopka, P., and Voges, E., 1999, "All-Solicon Bistable Micromechanical Fiber Switch Based on Advanced Bulk Micromaching", *IEEE Journal of Selected Topics in Quantum Electronics*, **5**, (1), 46-52.

[10] Redmond, S.M., Oliveira, S., and Rand, S.C., 2004,

”Bistablt Emission of a Blackbody Radiator”, *Appl. Phys. Lett.*, submitted.

[11] Lawandy, A.M., Balachandran, R.M., Gomes, A.S.L., and Sauvain, E., 1994, ”Laser Action in Strongly Scattering Media”, *Nature*, **368**, 436-437.

[12] Cao, H., Zhao, Y.G., Ho, S.T., Seelig, E.W., Wang, Q.H., and Chang, R.P.H., 1999, ”Random Laser Action in Semiconductor Powder”, *Phys. Rev. Lett.*, **82**, (11), 2278-2281.

[13] Zhang, Z.M., and Flik, M.I., 1993, ”Predicted Absorption of $YBa_2Cu_3O_7$/YSZ/Si Multilayer Structures for Infrared Detectors”, *IEEE Transactions on Applied Superconductivity*, **3**, (1), 1604-1607.

[14] Kong, J.A., 2000, *Electromagnetic wave theory*, EMW Publishing, Cambridge.

[15] Ruan, X.L., and Kaviany, M., 2004, ”Local Field Enhancement and Photon Localization in Monochromatically Irradiated, Random Porous Media”, *Microscale Thermophys. Engin.*, submitted.

[16] Hehlen, M.P., Gudel, H.U., Shu, Q., and Rand, S., 1995, ”Cooperative Optical Bistability in the Dimer System $Cs_3Y_2Br_9$:10%Yb^{3+}”, *J. Chem. Phys.*, **104**, (4), 1232-1244.

[17] Miyakawa, T., and Dexter, D.L., 1970, ”Phonon Sidebands, Multiphonon Relaxation of Excited States, and Phonon-Assisted Energy Transfer between Ions in Solids”, *Phys. Rev. B*, **1**, (7), 4069-4077.

[18] Costa, J., Roura, P., Morante, J.R., and Bertran, E., 1998, ”Blackbody Emission under Laser Excitation of Silicon Nanopowder Produced by Plasma-Enhanced Chemical-Vapor Deposition”, *J. Appl. Phys.*, **83**, (12), 7879-7885.

[19] Siegel, R., and Howell, J.R., 2002, *Thermal Radiation Heat Transfer, Fourth Edition*, Taylor & Francis, New York.

[20] Touloukian, Y.S., Ho, C.Y., 1970, *Thermophysical properties of matter, the TPRC data series; a comprehensive compilation of data*, IFI-Plenum, New York.

[21] Kaviany, M., 2002, *Principles of Heat Transfer*, Wiley, New York.

[22] Hecht, E., 2002, *Optics*, Addison Wesley, San Francisco.

[23] Schaack, G., Koningstein, J.A., 1970, ”Phonon and Electronic Raman Spectra of Cubic Rare-Earth Oxides and Isomorphous Yttrium Oxide”, *J. Opt. Soc. Am.*, **60**, (8), 1110-1115.

[24] Redmond, S., Rand, S.C., Ruan, X.L., and Kaviany, M., 2004, ”Multiple Scattering and Nonlinear Thermal Emission of Yb^{3+}, Er^{3+}:Y_2O_3 Nanopowders”, *J. Appl. Phys.*, **95**, (8), 2961-2969.